

Transparent fluids for 157-nm immersion lithography

Roderick R. Kunz

Michael Switkes

Roger Sinta

Jane E. Curtin

Massachusetts Institute of Technology

Lincoln Laboratory

Lexington, Massachusetts 02420-9108

Roger H. French

Robert C. Wheland

Chien-Ping Chai Kao

Michael P. Mawn

Lois Lin

DuPont Central Research and

Development

Wilmington, Delaware 19880-0356

Paula Wetmore

Val Krukoni

Kara Williams

Phasex Corporation

Lawrence, Massachusetts 01843

Abstract. More than 50 fluorocarbon liquids are measured for transparency over the wavelength range 150 to 200 nm for the purpose of identifying a suitably transparent fluid for use in 157-nm liquid immersion lithography. Purification methods such as degasification, distillation, silica gel drying, and supercritical fluid fractionation are investigated to determine the impact of residual contaminants on absorbance. The purification processes are monitored by gas chromatography-mass spectrometry and Fourier-transform infrared spectroscopy (for organics), ^{19}F -nuclear magnetic resonance spectroscopy (for molecular structure), gel permeation chromatography (for molecular weight), Karl Fisher analysis (for water), and for residual dissolved oxygen. We find that in most cases, the absorbance is dominated by dissolved oxygen and water. Once the contaminant levels are reduced, the most transparent perfluoroether (PFE) measured is perfluoro-1,2-bis(2-methoxyethoxy)ethylene glycol (perfluorotriglyme) at 0.52 cm^{-1} , the most transparent perfluoroalkane (PFA) measured is perfluorohexane at 1.1 cm^{-1} , the most transparent hydrofluoroether (HFE) was 1-(1H-tetrafluoro)ethoxy-2-(1-trifluoromethyl)tetrafluoroethoxy-2-trifluoromethyl-1,1,2-trifluoroethane at 2.6 cm^{-1} , and the lowest projected absorption coefficient for a hydrofluoroalkane (HFA) is decafluoro-2H,3H-pentane at $<2\text{ cm}^{-1}$. Our chemical analysis shows that some impurities still remain in these materials, and further reductions in absorption are likely. Even so, our current absorption values should allow lens-to-wafer working distances (assuming 95% transmission) of 428, 203, 83, and $111\text{ }\mu\text{m}$, respectively, for the four classes of fluids. The identification of these four classes (PFEs, PFAs, HFEs, and HFAs) of fluids for potential use as 157-nm immersion fluids, each with their own ranges of viscosity, vapor pressure, refractive index, dn/dT , synthetic routes, and cost, should allow for flexibility in performing tradeoff analyses for various 157-nm immersion lithography engineering designs and cost of ownership estimates. © 2004 Society of Photo-Optical Instrumentation Engineers. [DOI: 10.1117/1.1637366]

Subject terms: 157-nm lithography; immersion fluid; perfluoropolyether; transparency; fluorocarbon; fluoroether.

Paper 014013 received Aug. 4, 2003; revised manuscript received Oct. 16, 2003; accepted for publication Oct. 17, 2003.

1 Introduction

Immersion lithography, the practice of filling the lithographic lens-to-wafer gap with a transparent fluid, has been known for some time to provide a theoretical improvement in the achievable resolution for any given exposure wavelength.¹ Despite the well-recognized potential benefits, immersion lithography in practice has only very recently been considered seriously, and only at 193 nm, where the tool infrastructure is established and a convenient, transparent fluid is readily available (water).² Extension of immersion lithography to 157 nm requires not only the development of a 157-nm tool infrastructure, but the development of an inexpensive, transparent fluid. Recent work³ has shown that perfluorinated ethers provide the greatest transparency of any material at 157 nm, with absorption coefficients of the best deoxygenated perfluoropolyethers (PFPEs) of approximately 3 cm^{-1} . This value

limits the maximum lens working distance for 95% transmission through the fluid to only $\sim 75\text{ }\mu\text{m}$. For more practical working distances (WD), the absorption coefficient needs to be reduced, to 0.45 cm^{-1} for a 0.5-mm WD, and further to 0.22 cm^{-1} for a 1-mm WD. Clearly, improvements of nearly one order of magnitude are desired to warrant more serious consideration of 157-nm immersion lithography as a viable alternative. This work summarizes in detail the transparencies measured for a wide variety of fluorinated fluids, including, for comparison, those preliminary results that appear in Ref. 3.

As is shown, the absorption coefficients of these materials are often dominated by the amount of residual contaminants present. To give an idea of how important this is, Table 1 shows the added absorbance expected from a variety of common contaminants, given reported values^{4,5} of their absorption coefficients at 157.5 nm. These values in-

Table 1 A list of absorption coefficients for potential contaminants found in 157-nm immersion fluids. The right-most column shows the calculated contribution to absorbance should the contaminant be present at 1 ppm. (The organic solvent is a calculated value, assuming an absorption coefficient for polystyrene of $6 \mu\text{m}^{-1}$, a density of 1.1 g/cm^3 , and a molecular weight of 104 Da. This would be roughly equivalent to a value for an organic solvent such as toluene.)

Compound	Abs. coeff. ($\text{cm}^2/\text{molecule}$)	Ref.	Added absorbance/ppm (by wt)
O ₂	6.3×10^{-18}	4	0.20
H ₂ O	2.6×10^{-18}	4	0.15
CO ₂	2.2×10^{-19}	4	0.005
CFC solvent (CFCl ₂ CFCl ₂)	7.7×10^{-18}	5	0.0035
Organic solvent	1.0×10^{-17}		0.10

dicates that, for example, a perfectly transparent liquid containing 30-ppm oxygen, 10-ppm water, 5-ppm carbon dioxide, and 1 ppm of organic solvent, would exhibit an absorption coefficient of $\sim 7.6 \text{ cm}^{-1}$ from these impurities alone. To put these concentrations into perspective, the product literature⁶ for a common PFPE indicates that the solubility limit (at 1-atm) of oxygen in the fluid is ~ 52 ppm (36 cm^3 dissolved oxygen per 100 cm^3 liquid), and that of water in the fluid is 14 ppm. Without degasification and dehydration, we could then expect to see absorption coefficients no less than about 5 cm^{-1} when the fluid is exposed to air, even if the material were perfectly transparent. Other materials may exhibit solubility limits even greater than this. Quantifying these effects and determining the fundamental limiting absorbance for a variety of potential 157-nm immersion fluids is a central goal of the present work. However, there are additional requirements for these fluids that have not been addressed in this current work, including other optical properties such as absolute refractive indices, dn/dT , and dispersion ($dn/d\lambda$). These values will need to be determined to ultimately determine any liquid's utility as a 157-nm immersion fluid.

2 Experimental

2.1 Fluids Tested

Some of the materials evaluated in this study were custom synthesized, whereas others were commercially available. In particular, the perfluoro-1,2-bis(2-methoxyethoxy)ethylene glycol (also known as perfluorotriglyme) and perfluoro-15-crown-5 were custom synthesized via direct fluorination reaction at Exflor Chemical (Round Rock, Texas). The perfluorotriglyme was prepared from a solution of 1,2-bis(2-methoxyethoxy)ethylene glycol (triethylene glycol dimethyl ether, triglyme) in either hexafluoro-1,1,3,4-tetrachloro butane or 1,1,2-trichlorotrifluoroethane via introduction into a reactor (the design of which is described in U.S. Patent No. 5,093,432⁷) containing additional hexafluoro-1,1,3,4-tetrachloro butane, sodium fluoride, and saturated fluorine gas. A mixture of helium and fluorine gases was then flowed over the solution for 24 h. After purging with nitrogen, the product was isolated by distillation. The perfluoro-15-crown-5 was also

prepared via a similar direct fluorination process. All other materials were prepared internally at DuPont Corporation, except the following materials, which were obtained commercially. The Fluoroclean® HE was obtained from Castrol. The Solkane® 365, Galden® HT, and ZT series fluids, Perfluorosolv2® (PFS2), and Fomblin® Z and Y series fluids were all obtained from Solvay Solexis. A second sample of Perfluorosolv2® was obtained from SPI Chem, and the Demnum® S20 was obtained from Daikin.

2.2 Purification Procedures

Samples of the oligomeric and polymeric PFPEs Galden® HT-200, Fomblin® Z3, Fomblin® Z15, Fomblin® Z25, Fomblin® Z60, and Demnum® S20 were purified via supercritical carbon dioxide (CO₂) fractionation (SCF).⁸ In SCF fractionation, a sample can be separated into fractions whose solubilities vary slightly as a function of the supercritical fluid conditions. Each of the SCF purifications resulted in five fluid fractions of decreasing solubility in the supercritical CO₂. In general, the first fractions were composed of lowest boiling point, lowest molecular weight materials.

Alternative methods were used to purify selected fluorocarbon solvents. In general, only the most transparent, unpurified samples were selected for purification. The perfluorotriglyme was purified via standard distillation performed at atmospheric pressure using a 12-in. Vigreux column. Heat was supplied via a standard heating mantle, controlled so as to maintain a slow, steady flow of condensate (about 2 to 3 mL/min). The first fraction (10%) was collected between 95 to 105°C and discarded, the second fraction (80%) was collected at exactly 105°C (uncorrected). When the temperature began to change, the collection was stopped. The second fraction showed only a trace ($\ll 1$ ppm) of residual high boiling chlorinated impurities (as determined using analytical procedures described later) that absorb strongly at 157.5 nm. An alternative purification procedure was also used on the perfluorotriglyme, both as a stand-alone procedure and in conjunction with the distillation process. The alternative purification method used a short column of silica gel (4×0.5 in.), prepared by pouring dry silica into a glass tube. The fluorinated fluid was then introduced onto the top of the column and allowed to flow through its length. The first few percent of collected material was discarded and the next 60% was saved for analysis.

Water was removed from the liquids either by the silica column purification described earlier or direct immersion of 3A molecular sieves in the form of 8 to 12 mesh beads (EM Science MX 1583D-1). The sieves were activated by loading in a Hastelloy tube, heating to 300 to 500°C under nitrogen or air, cooling under nitrogen, and adding while still warm to the fluid to be dried. Alternatively, 3A molecular sieves were activated by baking at $\sim 200^\circ\text{C}$ under nitrogen for ~ 24 h in an oven. The latter procedure was used to maintain the dryness of fluids dried using the silica column procedure. Under a blanket of dry nitrogen, the dried fluids were then either decanted off the molecular sieves or filtered for separation from the molecular sieves immediately prior to measurement. Finally, two methods were used to remove dissolved gas. The first was used to displace both CO₂ and O₂ from the fluid, and involved bubbling a fine stream of dry N₂ through the sample for several minutes

Table 2 A summary of dissolved gas concentrations in selected fluorocarbon fluids. See the text for a description of the measurement and purification methods. The right-most column shows the calculated contribution to absorbance at 157.5 nm. Solubility of O₂ in Solkane® 365 mfc and CF₃CF₂CF₂OCF(CF₃)CF₂OCFHCF₃ were estimated from measured solubilities of N₂ in Solkane® 365 mfc at 25.12°C, and in CF₃CF₂CF₂OCF(CF₃)CF₂OCFHCF₃ at -15.5, 0.3, 50.28, and 59.6°C. Solubilities for CO₂ in Solkane® 365 mfc at 20°C was estimated from the data at -9.95°C, and solubility for CO₂ in CF₃CF₂CF₂OCF(CF₃)CF₂OCFHCF₃ at 20°C was estimated from the data at 50.12°C and -10.4°C. *Assumes oxygen present at >100 ppm. **Assumes water present at >50 ppm.

Fluid	O ₂ (ppm by wt)		CO ₂ (ppm by wt)		Water content (ppm by wt)			Added abs. due to gases calc'd (cm ⁻¹)	As rec'd abs. exp'l (cm ⁻¹)
	Under 14.7 psi O ₂	Under 3.07 psi O ₂	Under 14.7 psi CO ₂	Under 0.00485 psi CO ₂	As rec'd	Eq with H ₂ O	After dry		
CF ₃ CFHCFHCF ₂ CF ₃	461 (20°C)	97	5940 (17°C)	1.94	72		0.71	35	10
Perfluorohexane (<i>n</i> -C ₆ F ₁₄)	499 (17°C)	104	2900 (15°C)	0.95	5.5	9.1	<0.1	10	9
Solkane (CF ₃ CF ₂ CF ₂ CH ₃)	514 (25°C)	107	9100 (20°C)	2.9	218	706	12	37	33
CF ₃ CF ₂ CF ₂ OCF(CF ₃)CF ₂ OCFHCF ₃	451 (25°C)	91	3500 (20°C)	1.1	257		0.94	66	20
Perfluoro-N-methylmorpholine 3M® Performance Fluid PF-5052					5.2		2.6	>10	14
Perfluorooctane (<i>n</i> -C ₈ F ₁₈)		85						>20**	
CF ₃ CF ₂ CF ₂ OCFHCF ₃		127						>30**	76
HCF ₂ O(CF ₂ O) _n (CF ₂ CF ₂ O) _m CF ₂ H Galden® ZT 85					116		1.1	>20*	37

(i.e., sparging) while the sample was held under a nitrogen blanket. The second method involved complete degassing (including N₂) by placing the sample in a test tube bearing a stopcock, and then performing three freeze-evacuate-thaw cycles using a solvent-free all-dry vacuum pump. This latter method was effective at removing the N₂ and O₂, but did not effectively remove the CO₂. A summary of dissolved gas concentrations for selected fluids appears in Table 2, as do the estimates for absorbance at 157.5 nm that result from these gases. From both Tables 1 and 2, the importance of removing dissolved gases becomes very apparent.

2.3 Chemical Analysis Methods to Assess Fluid Purity

Following the purification of selected fluorocarbon fluids, the compositions of the fluids were evaluated to correlate with the VUV absorbance. For the organofluorine solvents, gas chromatography with mass spectrometric detection (GCMS) was performed using an Agilent 6890/5973 GCMS equipped with a 60-m-long low-bleed polydimethylsiloxane column. The initiation of the temperature ramp was at 7 min into the run, to maximize our ability to separate and detect low boiling point fluorocarbon impurities. The oligomeric and polymeric PFPEs that were fractionated using supercritical carbon dioxide were evaluated using ¹⁹F-nuclear magnetic resonance spectroscopy (NMR), gel permeation chromatography (GPC), and Fourier transform infrared spectroscopy (FTIR). The ¹⁹F-NMR was performed at Massachusetts Institute of Technology (MIT) using a Varian Mercury 300-MHz NMR; the GPC was

performed by American Polymer Standards and used Freon®113 (1,1,2-trichlorotrifluoroethane) with polystyrene standards; and the FTIR was performed at Lincoln Laboratory on a Bruker Equinox 55 FTIR.

Water analyses were performed by Karl Fischer coulometric titration using a Mettler DL37 KF Coulometer. HYDRANAL®-Coulomat AG and HYDRANAL®-Coulomat CG were used as the coulometric reagents. Additional solvent such as Freon®113 (1,1,2-trichlorotrifluoroethane) was added in instances of poor miscibility as, for example, between the coulometric reagents and perfluorohexane.

The results from all these tests were not only correlated to the absorption coefficients measured at 157.5 nm, but to any absorption bands observed in the vacuum ultraviolet region. This information led us to prioritize various types of contaminants with regard to their concentration, difficulty of removal, and contribution to absorption (i.e., not all the contaminants absorb most strongly at 157.5 nm).

2.4 Gas Solubility Measurements

The solubility of atmospheric gases in selected fluids was determined by recording the volume of gas that would dissolve into a previously gas-free fluid sample. The amount of dissolved gas was recorded by varying the isobaric headspace volume over the fluid.

A detailed description of the method is as follows. A 71-cm³ sapphire vapor liquid equilibrium (VLE) cell was first immersed in a constant temperature bath (a glass beaker filled with silicone oil). The bath temperature was controlled using a Eurotherm 2604 to ±0.01°C and measured

to the same accuracy using a Hart 1502A thermometer with a Hart 5614 RTD. The measurement procedure started by transferring 40 to 50 cm³ of pre-degassed solvent from its source cylinder to the evacuated VLE cell; the amount transferred was determined by weighing the source cylinder before and after the transfer. The gas was loaded first from its source cylinder into an HIP pump (High Pressure Equipment, Company positive displacement pump), whose shaft is driven by a computer-controlled stepper motor. The pump is kept at 24°C by circulating a constant temperature fluid through the insulated jackets using a Neslab circulating bath. After the pressure of the gas inside the HIP pump stabilized, the gas was loaded from the pump into the cell, and equilibrium cell pressure was measured. After each loading, the shaft was positioned such that the pressure of the gas in the HIP pump was the same as before the loading. Two Paroscientific quartz pressure transducers (model 31 K and 740-1 K) were used to measure the cell pressure and pump pressure, respectively. The amount of the gas loaded into the cell was calculated from the volume displacement of the shaft and the density of the gas at the pump temperature and pressure. For each solubility experiment, vapor pressure of the solvent as well as successive isothermal pressures for solutions of different gas concentrations are measured. In cases where oxygen data were not available, oxygen solubility was estimated from existing nitrogen data. It is unsafe to pressurize highly flammable fluids such as Solkane® with high pressure oxygen.

After the measurements were completed, the solvent (component 1) and gas (component 2) loadings were converted to equilibrium vapor and liquid phase compositions by accounting for the amount of each component in the vapor phase. The material balance equations for data reduction are:

$$n^L + n^V = n_1 + n_2, \quad (1)$$

$$n_1 = x_1 n^L + y_1 n^V, \quad (2)$$

$$V_T = n^L v^L + n^V v^V, \quad (3)$$

where n_i is the number of moles of component i charged to the cell, n^α is the total number of moles in phase α , v^α is the molar volume of phase α , x_1 and y_1 are the liquid and vapor mole fractions of component 1, and V_T is the total volume of the cell.

An expression for the number of moles in the liquid phase was derived from Eqs. (1) and (3):

$$n^L = [(n_1 + n_2)v^V - V_T]/(v^V - v^L). \quad (4)$$

An expression for the mole fraction of component 1 in liquid was derived from Eqs. (1) and (2):

$$x_1 = [n_1 - (n_1 + n_2 - n^L)y_1]/n^L. \quad (5)$$

A solution for x_1 was found at the temperature of interest by a conventional vapor-liquid equilibrium calculation, in which the equilibrium pressure and y_1 were first determined from the temperature and an initial estimate for x_1 . Equations (4) and (5) were then used to update the estimated value of x_1 . This iterative procedure is repeated until

x_1 converges to a single value. In this calculation, the vapor and liquid fugacities of each component, as well as v^L and v^V , are obtained from the Peng-Robinson equation of state⁹ with modified mixing rules¹⁰

$$P = RT/(v - b) - a/[v(v + b) + b(v - b)], \quad (6)$$

$$a = \sum \sum x_i x_j a_{ij},$$

$$a_{ij} = (a_{ii} a_{jj})^{1/2} [1 - (x_i K A_{ij} + x_j K A_{ji}) / (x_i + x_j)], \quad (7)$$

$$b = \sum \sum x_i x_j b_{ij}, \quad b_{ij} = (b_{ii} + b_{jj})/2. \quad (8)$$

Peng-Robinson equations of state (PREOS) parameters for a solvent, a_{11} and b_{11} , were obtained from vapor pressure and liquid density at each temperature of interest. PREOS parameters for a gas, a_{22} and b_{22} , were obtained from its acentric factor and critical properties as originally proposed by Peng and Robinson.⁹ At each temperature, the binary parameters $K A_{12}$ and $K A_{21}$ were obtained by minimizing $[1/N \sum (P_{\text{exp}}/P_{\text{calc}} - 1)^2]^{1/2}$. Once $K A_{12}$ and $K A_{21}$ are reduced from the measured solubility data, the solubilities of the gas at other pressures are calculated using PREOS.

2.5 Determination of Fluid Absorption Coefficients

2.5.1 Spectrophotometric cell for measuring liquids

The fluid absorption coefficients were determined using standard spectrophotometric liquid cells equipped with the following modifications: the windows were made of calcium fluoride, the o-rings used to prevent liquid leakage were made from Teflon-coated Viton, the spacer gaskets used to determine the liquid path length were made from Teflon and varied in thickness from 0.037 to 0.15 cm (a total of six different sized spacers were available), and the input and output ports housed stainless steel Luer fittings to allow for easy coupling to the injecting syringe. The syringes used to introduce the fluid were made only from glass and stainless steel. The spectrophotometer and all transmission measurements, as well as all sample introductions into and out of the liquid cell, were performed inside a nitrogen glove box.

2.5.2 Measurement procedure

All measurements reported here were derived from Beer's Law fits of absorbance versus path length, with a minimum of three and a maximum of five different path lengths employed, the latter determined by the thickness of the spacer gaskets. Since the calcium fluoride windows were found to vary in transmission from 80 to 85%, we used the same set of windows for all path lengths. This reduced the 1 σ residual error in our curve fits to generally less than about $\pm 5\%$. The vacuum ultraviolet (VUV) spectra we report in Figs. 1–13 were derived from a point-by-point Beer's Law fit at every wavelength between 150 and 200 nm, using 0.5-nm steps.

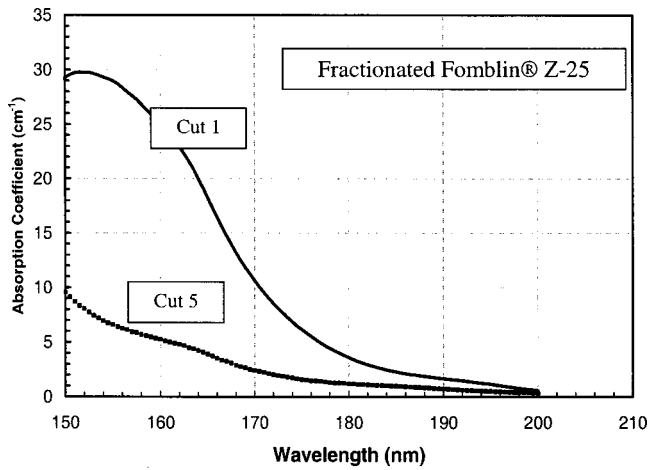


Fig. 1 Vacuum ultraviolet absorption spectra for two fractions of Fomblin Z purified using supercritical CO₂.

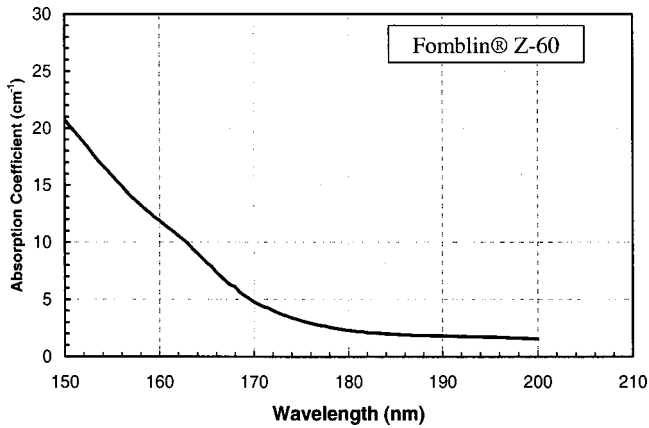


Fig. 2 Vacuum ultraviolet absorption spectra for undried Fomblin Z-60. Note the presence of the water absorption band at ~164 nm.

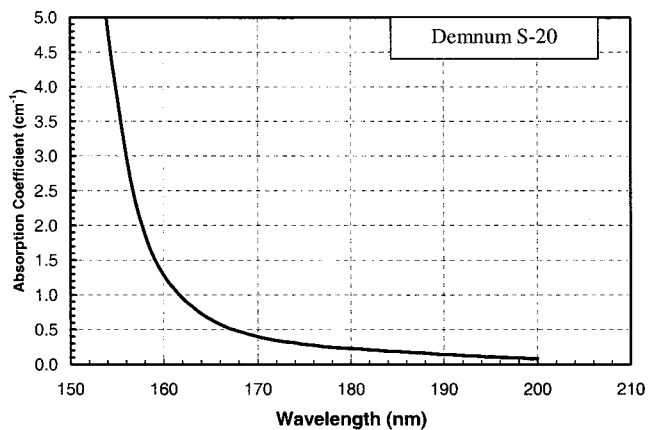


Fig. 3 Vacuum ultraviolet absorption spectra for dried Demnum S-20. The absorption coefficient at 157.5 nm is 2.1 cm⁻¹.

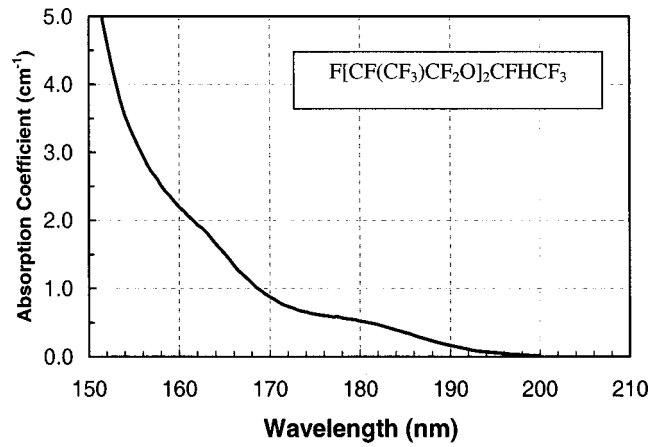


Fig. 4 Vacuum ultraviolet absorption spectra for the HFE F[CF(CF₃)CF₂O]₂CFHCF₃. Note the presence of acid fluoride contamination (as determined by GCMS) whose absorbance is at ~180 nm and, despite drying, a possible water absorption band at 164 nm.

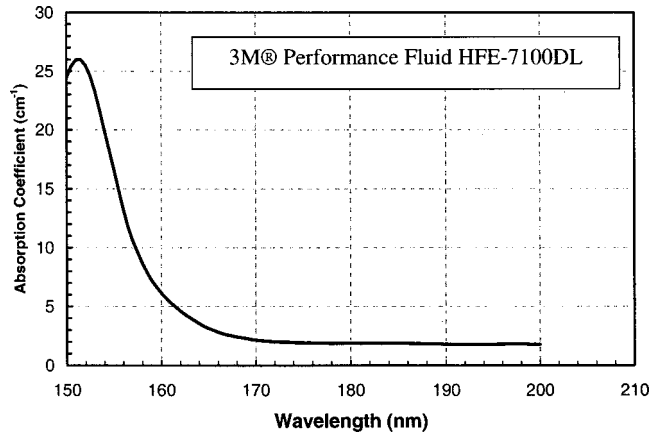


Fig. 5 Vacuum ultraviolet absorption spectra for the HFE comprised of a mixture of (CF₃)₂CFCF₂OCH₃ and CF₃CF₂CF₂CF₂OCH₃.

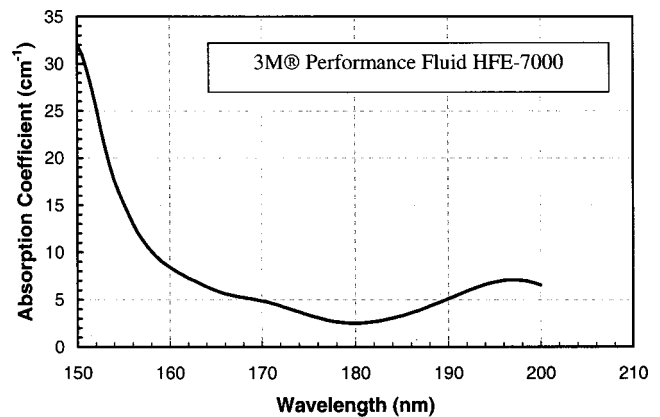


Fig. 6 Vacuum ultraviolet absorption spectra for the HFE CF₃CF₂CF₂OCH₃. Note the contaminant peak at ~195 nm.

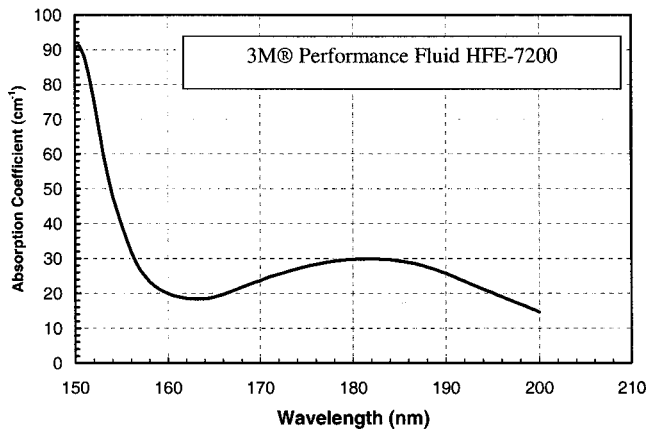


Fig. 7 Vacuum ultraviolet absorption spectra for the HFE comprised of a mixture of $(CF_3)_2CFCF_2OCH_2CH_3$ and $CF_3CF_2CF_2CF_2OCH_2CH_3$. Note the contaminant peak at ~ 180 nm.

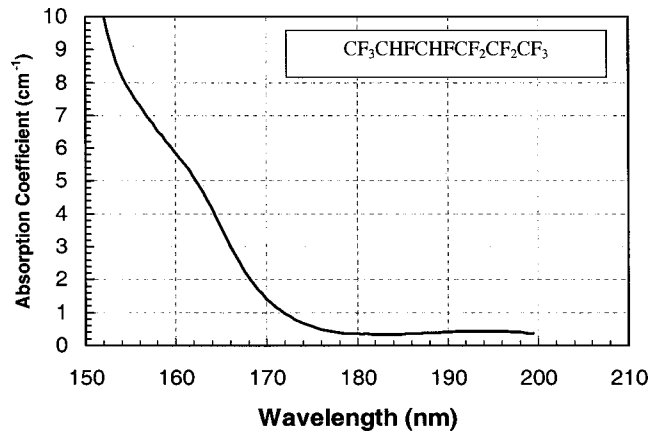


Fig. 10 Vacuum ultraviolet absorption spectra for the HFA $CF_3CHFCHF_2CF_2CF_2CF_3$ that is relatively pure (via GCMS) except for the remaining water that is apparent at 164 nm. Analysis of the spectrum in the absence of the contribution from water indicates the absorption coefficient of the purified material could be as low as 2 cm^{-1} .

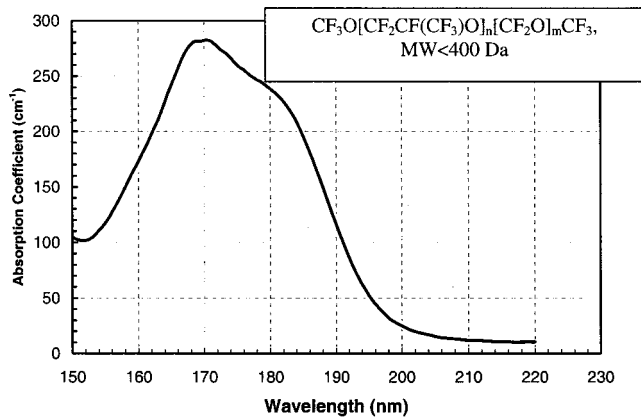


Fig. 8 Vacuum ultraviolet absorption spectra for the low molecular weight PFE solvent $CF_3O[CF_2CF(CF_3)O]_n[CF_2O]_mCF_3$ (MW < 400 Da). Note the huge contaminant absorbance due to a mixture of acid fluorides and/or alkenes. GCMS analysis of this material showed more than 50 different contaminants.

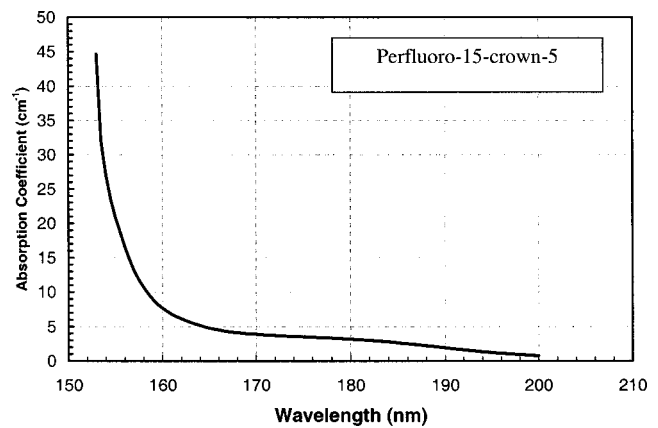


Fig. 11 Vacuum ultraviolet absorption spectra for the PFE perfluoro-15-crown-5 containing only a trace of chlorofluorocarbon solvent (via GCMS) and residual water.

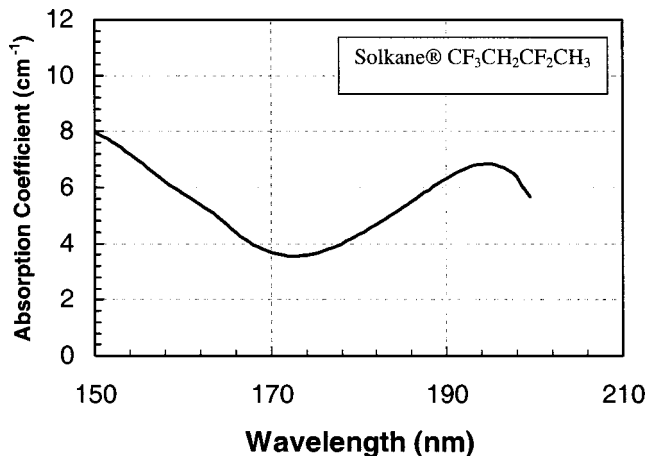


Fig. 9 Vacuum ultraviolet absorption spectra for the HFA $CF_3CH_2CF_2CH_3$ containing known contaminants comprised of unsaturated chlorofluorocarbons (see Table 7).

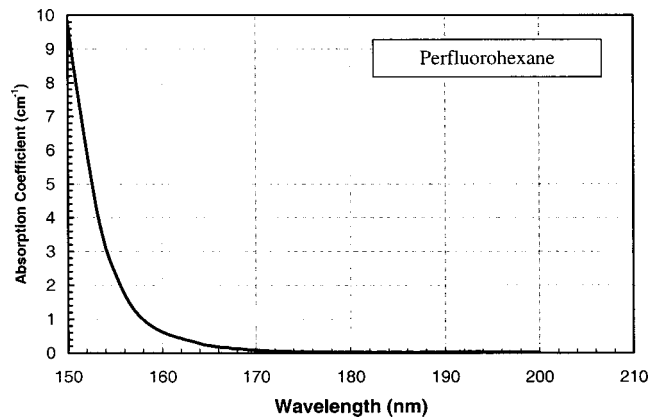


Fig. 12 Vacuum ultraviolet absorption spectra for purified perfluorohexane.

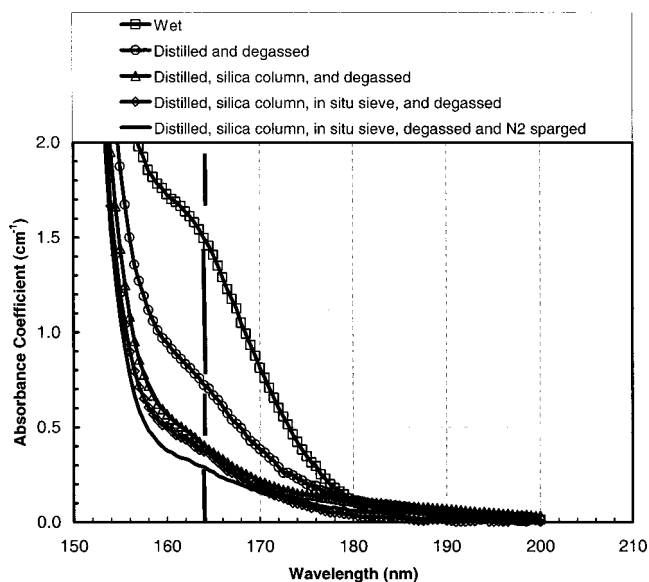


Fig. 13 Vacuum ultraviolet absorption spectra for various purities of perfluorotriglyme, where the principal contaminant affecting the absorbance is dissolved water. The solid vertical line indicates the approximate location of the λ_{\max} for water.

3 Results

Our approach was to first measure the absorption coefficient at 157.5 nm for each fluid as it was received, and if the value was greater than $\sim 25 \text{ cm}^{-1}$, no further measurements were made. For materials whose “as received” absorption coefficients at 157.5 nm were less than $\sim 25 \text{ cm}^{-1}$, the fluids were remeasured in the degassed state. From these, a few “champion” materials were selected for rigorous purification and analysis procedures. Tables 3–5 sum-

marize the absorption coefficients that were measured. The combination of data from these tables, along with the chemical analysis results, gave a clear indication of the potential for each material. For example, the PFPEs that were first reported³ as a champion material only showed slight improvements on supercritical fluid fractionation, and the resultant ¹⁹F-NMR analysis revealed a variety of chemical structures (see Table 6), such as $-(\text{CF}_2\text{CF}_2\text{CF}_2)-$ and $-(\text{CF}_2\text{CF}_2\text{CF}_2\text{CF}_2)-$, that are not purported to be idealized structures of the material. These structural differences showed only weak correlation to the absorption coefficients, adding further uncertainty to their relevance. We also observed FTIR absorption bands at ~ 2920 and $\sim 2850 \text{ cm}^{-1}$ among the various fractions that weakly correlate to the 157.5-nm absorbance (i.e., highest in the lowest molecular weight fractions), indicating possible contamination from hydrocarbons. At this point, it is unclear whether these IR absorption bands arise from some external contaminant or some structural attribute of the polymer. However, given the challenge associated with identification and removal of the full list of potential absorbing moieties, it appears as though the commercially available PFPE oils may be costly and difficult to purify for use as immersion fluids at absorption coefficients less than 2 cm^{-1} .

As an alternative approach, we have identified a highly pure, low molecular weight version of a PFPE, perfluoro-1,2-bis(2-methoxyethoxy)ethylene glycol (perfluorotriglyme), that can be prepared $>98\%$ isomerically pure and $>99.9\%$ perfluoroether. Small amounts of residual contamination can be removed via a combination of distillation and silica gel purification, and, after complete purification, the material exhibits the lowest absorbance of anything measured to date at 0.52 cm^{-1} (Table 3). Based on our GCMS analysis of this material, it may be possible to reduce this absorbance only a small amount more, as a trace

Table 3 A summary of absorption coefficients (cm^{-1}) for low boiling point fluorocarbon solvents. Note that the differences in absorption coefficients for the degassed and dried perfluorotriglyme may be due to residual carbon dioxide.

SOLVENTS	Chemical structure or IUPAC name	As rec'd	Degas only	Dried and degassed
Perfluoro-triglyme	$\text{CF}_3\text{O}(\text{CF}_2\text{CF}_2\text{O})_3\text{CF}_3$	5.8	1.2	0.52 (N_2 sparge) 0.65 (vac degas)
	Perfluorohexane ($n\text{-C}_6\text{F}_{14}$)	9	1.6	1.1
3M® Performance Fluid HFE-7000	$\text{CF}_3\text{CHFCHFCF}_2\text{CF}_3$	10.0	6.8	
	$\text{CF}_3\text{CF}_2\text{CF}_2\text{OCH}_3$		8.1	
3M® Performance Fluid HFE-7100DL	$(\text{CF}_3)_2\text{CFCF}_2\text{OCH}_3 + \text{CF}_3\text{CF}_2\text{CF}_2\text{CF}_2\text{OCH}_3$		9.6	
	Perfluoro-15-crown-5, Lot 1, $c\text{-}(\text{CF}_2\text{CF}_2\text{O})_5$		14.3	
	Perfluoro-15-crown-5, Lot 2, $c\text{-}(\text{CF}_2\text{CF}_2\text{O})_5$		11.7	
3M® Performance Fluid PF-5052	Perfluoro-N-methylmorpholine $\text{O}(\text{CF}_2\text{CF}_2)_2\text{NCF}_3$	14		
	1,1,1,2,2,3,3,4,4-nonafluorohexane ($n\text{-C}_6\text{H}_5\text{F}_9$)	22		
3M® Performance Fluid HFE-7200	$(\text{CF}_3)_2\text{CFCF}_2\text{OCH}_2\text{CH}_3 + \text{CF}_3\text{CF}_2\text{CF}_2\text{CF}_2\text{OCH}_2\text{CH}_3$	26.4	22	
Solkane 365	$\text{CF}_3\text{CH}_2\text{CF}_2\text{CH}_3$	33	6.3	
	Perfluoroheptane ($n\text{-C}_7\text{F}_{16}$)	33.4		

Table 4 A summary of absorption coefficients (cm^{-1}) for oligomeric perfluoropolyethers.

PFPE oligomers	Chemical structure or IUPAC name	As rec'd	Degas only	Dried and degassed
Galden® HT-55	$\text{CF}_3\text{O}[\text{CF}_2\text{CF}(\text{CF}_3)\text{O}]_n[\text{CF}_2\text{O}]_m\text{CF}_3$, MW=340 Da		120	
Galden® HT-110	$\text{CF}_3\text{O}[\text{CF}_2\text{CF}(\text{CF}_3)\text{O}]_n[\text{CF}_2\text{O}]_m\text{CF}_3$, MW=580 Da	61.0		
Galden® HT-200 SCF cut 1	$\text{CF}_3\text{O}[\text{CF}_2\text{CF}(\text{CF}_3)\text{O}]_n[\text{CF}_2\text{O}]_m\text{CF}_3$, MW<870 Da	14.5		
Galden® HT-200 SCF cut 5	$\text{CF}_3\text{O}[\text{CF}_2\text{CF}(\text{CF}_3)\text{O}]_n[\text{CF}_2\text{O}]_m\text{CF}_3$, MW>870 Da	13.3		
Galden® ZT-85	$\text{HCF}_2\text{O}(\text{CF}_2\text{O})_m(\text{CF}_2\text{CF}_2\text{O})_n\text{CF}_2\text{H}$	37		
SPI Chem PFS2	$\text{CF}_3\text{O}[\text{CF}_2\text{CF}(\text{CF}_3)\text{O}]_n[\text{CF}_2\text{O}]_m\text{CF}_3$, MW<400 Da		44.5	
Fluoroclean® HE	$\text{CF}_3\text{O}[\text{CF}_2\text{CF}(\text{CF}_3)\text{O}]_n[\text{CF}_2\text{O}]_m\text{CF}_3$, MW<400 Da		144	
	$\text{F}[\text{CF}(\text{CF}_3)\text{CF}_2\text{O}]_1\text{CFHCF}_3$	76		
	$\text{F}[\text{CF}(\text{CF}_3)\text{CF}_2\text{O}]_2\text{CFHCF}_3$	20	9.2	2.6
	$\text{F}[\text{CF}(\text{CF}_3)\text{CF}_2\text{O}]_3\text{CFHCF}_3$	24		
	$\text{F}[\text{CF}(\text{CF}_3)\text{CF}_2\text{O}]_4\text{CFHCF}_3$	22		
	$\text{F}[\text{CF}(\text{CF}_3)\text{CF}_2\text{O}]_5\text{CFHCF}_3$	22		
	$\text{F}[\text{CF}(\text{CF}_3)\text{CF}_2\text{O}]_9\text{CFHCF}_3$	12		

Table 5 A summary of absorption coefficients (cm^{-1}) for perfluoropolyethers.

PFPE oils	Chemical structure or IUPAC name	As rec'd	Degas only	Dry only
Krytox® K9	$\text{CF}_3\text{O}[\text{CF}_2\text{CF}(\text{CF}_3)\text{O}]_n\text{CF}_3$	11.1		7
Krytox® K8	$\text{CF}_3\text{O}[\text{CF}_2\text{CF}(\text{CF}_3)\text{O}]_n\text{CF}_3$	17.3		
Fomblin® M15	$\text{CF}_3\text{O}[\text{CF}_2\text{CF}(\text{CF}_3)\text{O}]_n[\text{CF}_2\text{O}]_m\text{CF}_3$, Mw~8,000	16.3		
Fomblin® Z3 parent	$\text{CF}_3\text{O}(\text{CF}_2\text{CF}_2\text{O})_n(\text{CF}_2\text{O})_m\text{CF}_3$, Mw~4,000	16.8	15.6	
Fomblin® Z3 SCF cut 1	$\text{CF}_3\text{O}(\text{CF}_2\text{CF}_2\text{O})_n(\text{CF}_2\text{O})_m\text{CF}_3$,		21.5	
Fomblin® Z3 SCF cut 5	$\text{CF}_3\text{O}(\text{CF}_2\text{CF}_2\text{O})_n(\text{CF}_2\text{O})_m\text{CF}_3$,		11.5	
Fomblin® Z15	$\text{CF}_3\text{O}(\text{CF}_2\text{CF}_2\text{O})_n(\text{CF}_2\text{O})_m\text{CF}_3$, Mw~8,000	21.8		
Fomblin® Z25 parent	$\text{CF}_3\text{O}(\text{CF}_2\text{CF}_2\text{O})_n(\text{CF}_2\text{O})_m\text{CF}_3$, Mw~9,500	19.3	17.3	
Fomblin® Z25 SCF cut 1	$\text{CF}_3\text{O}(\text{CF}_2\text{CF}_2\text{O})_n(\text{CF}_2\text{O})_m\text{CF}_3$,		27.3	
Fomblin® Z25 SCF cut 2	$\text{CF}_3\text{O}(\text{CF}_2\text{CF}_2\text{O})_n(\text{CF}_2\text{O})_m\text{CF}_3$,		23.1	
Fomblin® Z25 SCF cut 4	$\text{CF}_3\text{O}(\text{CF}_2\text{CF}_2\text{O})_n(\text{CF}_2\text{O})_m\text{CF}_3$,		17.1	
Fomblin® Z25 SCF cut 5	$\text{CF}_3\text{O}(\text{CF}_2\text{CF}_2\text{O})_n(\text{CF}_2\text{O})_m\text{CF}_3$,		5.9	
Fomblin® Z60 parent	$\text{CF}_3\text{O}(\text{CF}_2\text{CF}_2\text{O})_n(\text{CF}_2\text{O})_m\text{CF}_3$, Mw~13,000	12.8	5.8	
Fomblin® Z60 SCF cut 1	$\text{CF}_3\text{O}(\text{CF}_2\text{CF}_2\text{O})_n(\text{CF}_2\text{O})_m\text{CF}_3$,		11.4	
Fomblin® Z60 SCF cut 4	$\text{CF}_3\text{O}(\text{CF}_2\text{CF}_2\text{O})_n(\text{CF}_2\text{O})_m\text{CF}_3$,		4.6	
Fomblin® Z60 SCF cut 5	$\text{CF}_3\text{O}(\text{CF}_2\text{CF}_2\text{O})_n(\text{CF}_2\text{O})_m\text{CF}_3$,		4.7	
Fomblin® Y18 SCF cut 1	$\text{CF}_3\text{O}[\text{CF}_2\text{CF}(\text{CF}_3)\text{O}]_n[\text{CF}_2\text{O}]_m\text{CF}_3$	14.9		
Fomblin® Y18 SCF cut 4	$\text{CF}_3\text{O}[\text{CF}_2\text{CF}(\text{CF}_3)\text{O}]_n[\text{CF}_2\text{O}]_m\text{CF}_3$	8.7		
Demnum® S20 Parent	$\text{CF}_3\text{O}(\text{CF}_2\text{CF}_2\text{CF}_2\text{O})_n\text{CF}_3$	10.5	3.1 (degas)	6 (no degas)
Demnum® S20 Parent (con't)	$\text{CF}_3\text{O}(\text{CF}_2\text{CF}_2\text{CF}_2\text{O})_n\text{CF}_3$		2.9 (N_2 sparge)	2.1 (with degas)
Demnum® S20 SCF cut 1	$\text{CF}_3\text{O}(\text{CF}_2\text{CF}_2\text{CF}_2\text{O})_n\text{CF}_3$	10.6		
Demnum® S20 SCF cut 5	$\text{CF}_3\text{O}(\text{CF}_2\text{CF}_2\text{CF}_2\text{O})_n\text{CF}_3$	10.2		

Table 6 ^{19}F -NMR and GPC analysis of the perfluoropolyethers that were purified by supercritical CO_2 fractionation. Note that the molecular weight values obtained by gel permeation chromatography (GPC) used polystyrene as a reference. The molecular values obtained from end-group NMR analysis are more accurate, but the error bars are larger due to limited signal to noise at high molecular weights. The absorption coefficient values (right-most column) are for degassed, but not dehydrated, samples.

	M_w (Vendor)	M_n (GPC)	M_w (GPC)	M_w/M_n (GPC)	M_w (NMR)	$\text{CF}_2\text{CF}_2\text{O}$ (NMR)	OCF_2 (NMR)	OCF_3 (NMR)	$(\text{CF}_2)_3$ (NMR)	$(\text{CF}_2)_4$ (NMR)	Abs (157.5nm)
Z03	4,000				4400	49.7	39.1	4.5	4.6	1.9	15.6
Cut 1					2430	49.8	35.7	8.2	4.7	1.5	21.5
Cut 2					3230	49.1	38.6	6.1	4.8	1.4	
Cut 3					3940	44.0	42.1	5.0	6.6	2.3	
Cut 4					6710	48.5	42.1	2.9	5.4	1.1	
Cut 5		71,000	79,150	1.06	17,200	47.3	47.0	1.1	4.3	0.3	11.5
Z25	9,500	29,350	44,400	1.22	4570	35.4	42.0	4.5	16.4	1.7	17.3
Cut 1		18,000	18,950	1.05	1970	28.2	47.3	9.9	12.9	1.6	27.3
Cut 2		20,700	21,650	1.05							23.1
Cut 3		25,150	27,550	1.05							
Cut 4		33,150	37,200	1.06							17.1
Cut 5		50,600	58,200	1.07	11,100	41.7	55.2	1.6	1.1	0.3	5.9
Z60	13,000				17,300	44.6	49.4	1.1	3.8	1.1	5.8
Cut 1					11,100	41.7	55.2	1.6	1.2	0.4	11.4
Cut 2						46.6	47.0	0.6	1.1	1.9	
Cut 3						47.8	47.0	0.0	3.9	1.1	
Cut 4					19,400	45.7	46.9	1.0	5.1	1.3	4.6
Cut 5						47.3	46.5	1.3	2.1	1.4	4.7

of residual solvent is still detected, so this at present is our limiting transparency at an absorption coefficient of $\sim 0.5 \text{ cm}^{-1}$.

Another class of materials has been identified whose absorption coefficient is only 1.1 cm^{-1} . We evaluated a purified form of perfluorohexane (>95% perfluorohexane/perfluorobutylethyl ether mixture, <0.1% unsaturated compounds by GCMS) and found that, after drying and degasification, the resulting absorbance was much lower than expected based on earlier, unpublished results. Additionally, the most transparent hydrofluoroether

we have measured is 1-(1H-tetrafluoro)ethoxy-2-(1-trifluoromethyl)tetrafluoroethoxy-2-trifluoromethyl-1,1,2-trifluoroethane at 2.6 cm^{-1} , and the lowest projected absorption coefficient for a hydrofluoroalkane (HFA) was decafluoro-2H,3H-pentane at $<2 \text{ cm}^{-1}$ (we were unsuccessful at our attempt to remove dissolved water, but have made this estimate based on spectral subtraction of water from its spectrum). Table 7 provides a partial summary of our GCMS analyses on the low molecular weight solvents and their hydrocarbon and/or halocarbon impurities,

Table 7 A list of the known hydrocarbon and halocarbon impurities detected via GCMS in various materials whose absorbances appear in Tables 3 and 4. *Residual dissolved water not removed.

Fluid class	Fluid	Abs. coeff. (cm^{-1})	Impurities
PFE	Perfluorotriglyme	0.52	$\text{CFCl}_2\text{CF}_2\text{CClFCF}_2\text{Cl}$ (0.01%) +trace of siloxanes from shipping-bottle caps
PFE	Perfluoro-15-crown-5	11.7*	$\text{CFCl}_2\text{CF}_2\text{CClFCF}_2\text{Cl}$ +related compounds (0.1%) $\text{C}_4\text{F}_9\text{OC}_2\text{F}_5$ (6.7%) C_6HF_{13} (0.46%)
PFA	Perfluorohexane ($n\text{-C}_6\text{F}_{14}$)	1.1	$n\text{-C}_4\text{F}_{10}$ (0.17%) $\text{CH}_2=\text{CHCF}_2\text{CF}_2\text{CF}_2\text{CF}_3$ (0.07%) +other related compounds
HFE	$\text{F}[\text{CF}(\text{CF}_3)\text{CF}_2\text{O}]_2\text{CFHCF}_3$	2.6	Various acid fluorides (0.29%)
HFA	$\text{CF}_3\text{CHFCHFCF}_2\text{CF}_3$	6.8*	Other $\text{C}_5\text{H}_2\text{F}_{10}$ compounds (0.36%) $\text{CF}_3\text{CF}=\text{CH}_2\text{CH}_2\text{CF}_2\text{CF}_3$ (0.01%)
HFA	$\text{CF}_3\text{CH}_2\text{CF}_2\text{CH}_3$	6.3*	$\text{CH}_2\text{ClCH}=\text{CHCF}_3$ + related compounds (0.47%)

Table 8 A summary of the most transparent fluorocarbon fluids at 193 nm. *These values can vary significantly depending on chain length. For example, perfluorotetraglyme, perfluoropentaglyme, etc. would be expected to exhibit higher viscosities and lower vapor pressures. Estimates using the Clausius-Clapeyron equation, the measured boiling point of 100°C, and an estimate of 8 to 9 kcal/mole for the heat of vaporization.

	Perfluorohexane at 157.5 nm	Perfluorotriglyme at 157.5 nm	Perfluorotriglyme at 193.4 nm	Water at 193.4 nm
Absorption coefficient (cm ⁻¹)	1.1	0.52	0.026	0.036 (Ref. 2)
Refractive index	Not measured, likely 1.35 to 1.40	~1.37	Not measured, likely 1.30 to 1.35	1.44
Absolute viscosity (cP)	<1		<1*	1.0
Vapor pressure at 21 °C (Torr)	232		Between 28 and 58 Torr*	20

whereas Figs. 1–13 show individual absorption spectra for selected materials listed in Tables 3–5.

4 Discussion

Since we have identified fluids that, in principle, enable 157-nm immersion lens designs with working distances between 0.2 and 0.5 mm, it now becomes instructive to take a closer look at the cost the immersion fluid would have on the operation of such a system. Although we acknowledge that such cost estimates may be speculative at this point, we must also note that perfluorinated fluids are performance materials with high capital cost. Currently, PFEs and PFAs can be purchased from a number of suppliers for \$75 to \$200 per liter, and HFAs for \$15 to \$50 per liter. Although the HFAs and HFEs may be less expensive, the absorbance results suggest we may be limited to using either the PFEs or the PFAs. Since use of any of these materials will require additional purification, we can estimate that the immersion fluid would cost near the upper limit of the current cost range, or about \$200 per liter. If we assume that each wafer will require a few tens of cubic centimeters of fluid, then with no fluid recycling, this would lead to a fluid cost of a few dollars per wafer level.

However, recent damage studies in our laboratory on perfluorotriglyme indicate the photon-induced darkening rate at 157.5 nm to be 0.0057 cm⁻¹ per J/cm² of exposure. This means that, for a 0.4-mm working distance and an initial absorption coefficient of 0.52 cm⁻¹, the starting transmission will be 95.3%, and it will not reach 95% until ~6 J/cm² of exposure. If we assume each field exposes the fluid to an incident dose of ~20 mJ/cm², then in principle the fluid could be used for ~300 exposure fields, based on transmission limited only by photon-induced darkening and not by photoresist outgassing. Development of a closed-loop recirculation system equipped with a purification capability to remove photoresist contaminants might allow the fluid to be effectively used >100 times, reducing the cost per wafer level to a few cents, which is now only a small fraction of the total cost per wafer level of >\$30.¹¹ Although we acknowledge that these figures represent rough estimates, they nevertheless point out that fluid radiation durability and clever engineering solutions that en-

able recycling of fluid within a tool will undoubtedly become critical aspects to any cost-effective implementation of 157-nm immersion lithography.

5 Comparison to Fluids Used for 193-nm Immersion

Immersion lithography at 193 nm is currently under development,² and the fluid of choice, based on initial studies, is pure water. The absorption coefficient of water³ at 193 nm is 0.036 cm⁻¹. One possible concern in the use of water would be its corrosive impact on materials such as the lens optics. If, for any reason, an alternative fluid is needed for 193-nm immersion lithography, the materials described in this current work would offer a good alternative. Table 8 lists the most transparent materials measured at 193 nm, and a comparison of their properties to those of water. The most noticeable difference is that these fluorinated fluids exhibit much higher vapor pressure than water, and readily evaporate at room temperature. It is important to point out that the perfluorinated ethers such as perfluorotriglyme (a trimer of perfluorinated ethylene glycol) can be prepared at different molecular weights (i.e., an “*n*-mer” of perfluorinated ethylene glycol) with correspondingly higher boiling points, vapor pressures, and viscosities, but with little impact on their transparency. This flexibility will undoubtedly need to be exploited to provide a fluid with optimal properties.

6 Summary

We have performed a rigorous assessment of the availability of transparent fluids for 157-nm immersion lithography and have found four classes of materials, notably the perfluoroethers, perfluoroalkanes, hydrofluoroethers, and hydrofluoroalkanes. The champion materials from each class exhibit absorption coefficients at 157.5 nm of 0.5, 1.1, 2.6, and <2 cm⁻¹, respectively, the latter two values still limited by known and quantified impurities. In performing these studies, we have identified dissolved O₂, H₂O, and CO₂ as primary sources of residual contamination, and several purification schemes are reported. This bodes well for development of fluids that can meet transparency specifications, without the need for rigorous separation and purifi-

cation of residual organics and solvents, but rather with an incorporation of a degassing system into the lithographic tool to perform the most important purification steps *in situ*, thereby enabling recycling and reducing the cost impact of using nonaqueous immersion fluids. Based on an estimated fluid cost of \$200/liter and initial laser-induced darkening experiments, it seems reasonable that a recirculation system that enables the fluid to be reused for many (>100) exposure fields will be both necessary and possible to reduce the cost impact of the fluid.

Finally, we must point out that other factors such as the fluids' potential to contribute to global greenhouse warming, their environmental persistence, and the status of their regulatory approval, will all ultimately impact the timing and economic model for use of these fluids in 157-nm immersion lithography.

Acknowledgments

This work was sponsored in part by the Advanced Lithography Program of the Defense Advanced Research Projects Agency under Air Force contract F19628-00-C-0002, and in part by a Cooperative Research and Development Agreement between MIT-Lincoln Laboratory and the E. I. Du Pont Demours Corporation. Opinions, interpretations, conclusions, and recommendations are those of the authors, and do not necessarily represent the view of the United States Government.

References

1. H. Kawata, J. M. Carter, A. Yen, and H. I. Smith, *Microelectron. Eng.* **9**, 31 (1989).
2. S. Owa and H. Nagasaka, "Immersion lithography: Its potential performance and issues," *Proc. SPIE* **5040**, 724–733 (2003).
3. M. Switkes, R. R. Kunz, R. F. Sinta, M. Rothschild, P. M. Gallagher-Wetmore, V. J. Krukoni, and K. Williams, "Immersion liquids for lithography in the deep ultraviolet," *Proc. SPIE* **5040**, 690–699 (2003); M. Switkes and M. Rothschild, "Resolution enhancement of 157-nm lithography by liquid immersion," *J. Microlithogr., Microfabr., Microsyst.* **1**, 225–228 (2002).
4. H. Okabe, *Photochemistry of Small Molecules*, John Wiley and Sons, New York (1978).
5. J. M. Dumas, P. Dupuis, G. Pfister-Guillouzo, and C. Sandorfy, "Ionization potentials and ultraviolet absorption spectra of fluorocarbon anesthetics," *Can. J. Spectrosc.* **26**(3), 102–108 (1981).
6. "Fomblin PFPE fluid gas solubility," product data sheet from Solvay Solexis, Bollate, Italy (2001).
7. "Liquid phase fluorination," U.S. Patent No. 5,093,432, issued to Ex-fluor Research Corporation (1992).
8. M. A. McHugh and V. J. Krukoni, *Supercritical Fluid Extraction: Principles and Practice*, Butterworth-Heinemann, Boston (1994).
9. D.-Y. Peng and D. B. Robinson, "A new two-constant equation of state," *Ind. Eng. Chem. Fundam.* **15**, 59–64 (1976).
10. C. P. Chai Kao, M. E. Paulaitis, and A. Yokozeki, "Double Azeotropy in Binary Mixtures of NH₃ and CHF₂CF₃," *Fluid Phase Equilib.* **127**, 191–203 (1997).
11. See <http://www.semtech.org/public/resources/litho/coo>.

Biographies and photographs of the authors not available.